Effect of Supramolecular Complexation of Alkali Hydrogenselenates with Crown Ethers and solid-solutions with their Hydrogensulfate Counterparts on the Solid-Solid Phase Transition Behaviors

*Samet Ocak,[a,b] Dario Braga,[a] Simone d'Agostino[a,]**

[a] The University of Bologna - Department of Chemistry "Giacomo Ciamician", Via F. Selmi 2, 40126, Bologna (BO), 40126, Italy.

[b] Current address: Institute for Microelectronics and Microsystems - Research National Council (IMM-CNR), Via Pietro Gobetti 101, 40129, Bologna (BO), Italy.

Table of contents	Page

Table ESI-1. Crystal data and refinement details for: **[18-crown-6·K]$HSeO_4 \cdot 2H_2O$**, **[18-crown-6·Rb]$HSeO_4 \cdot H_2O$**, **[18-crown-6·Cs]$HSeO_4 \cdot H_2O$**, **[18-crown-6·K]$HSeO_4$**, and the solid solution **[18-crown-6·K]$(HSeO_4)_{0.5}(HSO_4)_{0.5}$**.

	[18-crown-6·K] $HSeO_4 \cdot 2H_2O$	**[18-crown-6·Rb] $HSeO_4 \cdot H_2O$**	**[18-crown-6·Cs] $HSeO_4 \cdot H_2O$**	**[18-crown-6·K] $HSeO_4$**	**[18-crown-6·K] $(HSeO4)_{0.5}(HSO_4)_{0.5}$**
Formula	$C_{12}H_{25}KO_{10}Se \cdot 2(H_2O)$	$C_{12}H_{25}O_{10}RbSe \cdot H_2O$	$C_{12}H_{24}CsO_{11}Se \cdot H_2O$	$C_{12}H_{24}KO_{11}Se$	$C_{12}H_5KO_{11}Se_{0.5}S_{0.5}$
FW (g/mol)	483.41	511.76	556.18	447.38	423.93
Cryst. Sys.	Monoclinic	Monoclinic	Monoclinic	Monoclinic	Monoclinic
Space Group	Cc	*C2/c*	I2/a	$P2_1/n$	$P2_1/n$
a/Å	14.4882(5)	22.1681(14)	23.7101(16)	10.3653(5)	10.3093(8)
b/Å	17.5369(5)	9.9047(4)	8.4597(7)	8.5649(6)	8.5230(6)
c/Å	8.4421(3)	20.5896(12)	21.3553(18)	21.5820(14)	21.5977(15)
α/°	90	90	90	90	90
β/°	100.351	117.183	109.486	100.137(5)	99.684(7)
γ/°	90	90	90	90	90
Volume/Å^3	2110.04(12)	4021.5(5)	4038.1(6)	1886.1(2)	1870.7(2)
Z	4	8	8	4	4
ρ_{calc} g/cm^3	1.522	1.691	1.83	1.576	1.505
μ/mm^{-1}	2.03	4.32	3.69	2.256	1.358
measd rflns	4271	8182	8935	8987	8510
indep rflns	2952	4533	4576	4269	4312
R_1	0.054	0.05	0.079	0.0998	0.0800
wR_2	0.145	0.074	0.189	0.2103	0.1624

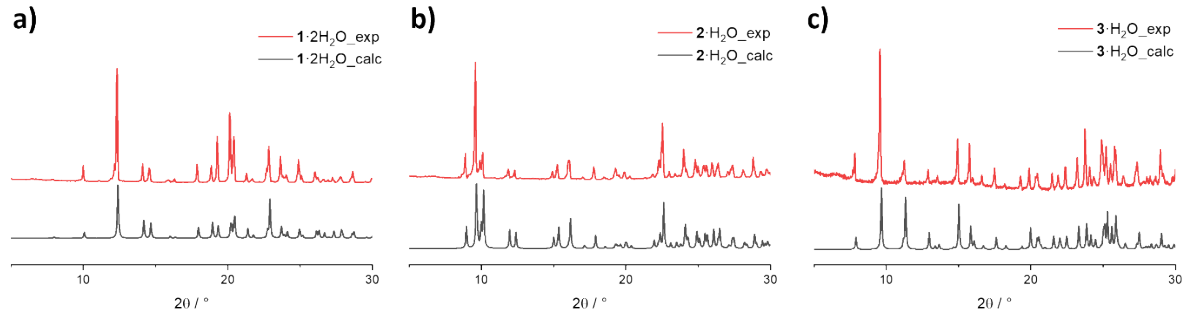

Figure ESI-1. Comparisons of calculated and experimental powder patterns: a) **1**·2H_2O, b) **2**·H_2O, and c) **3**·H_2O.

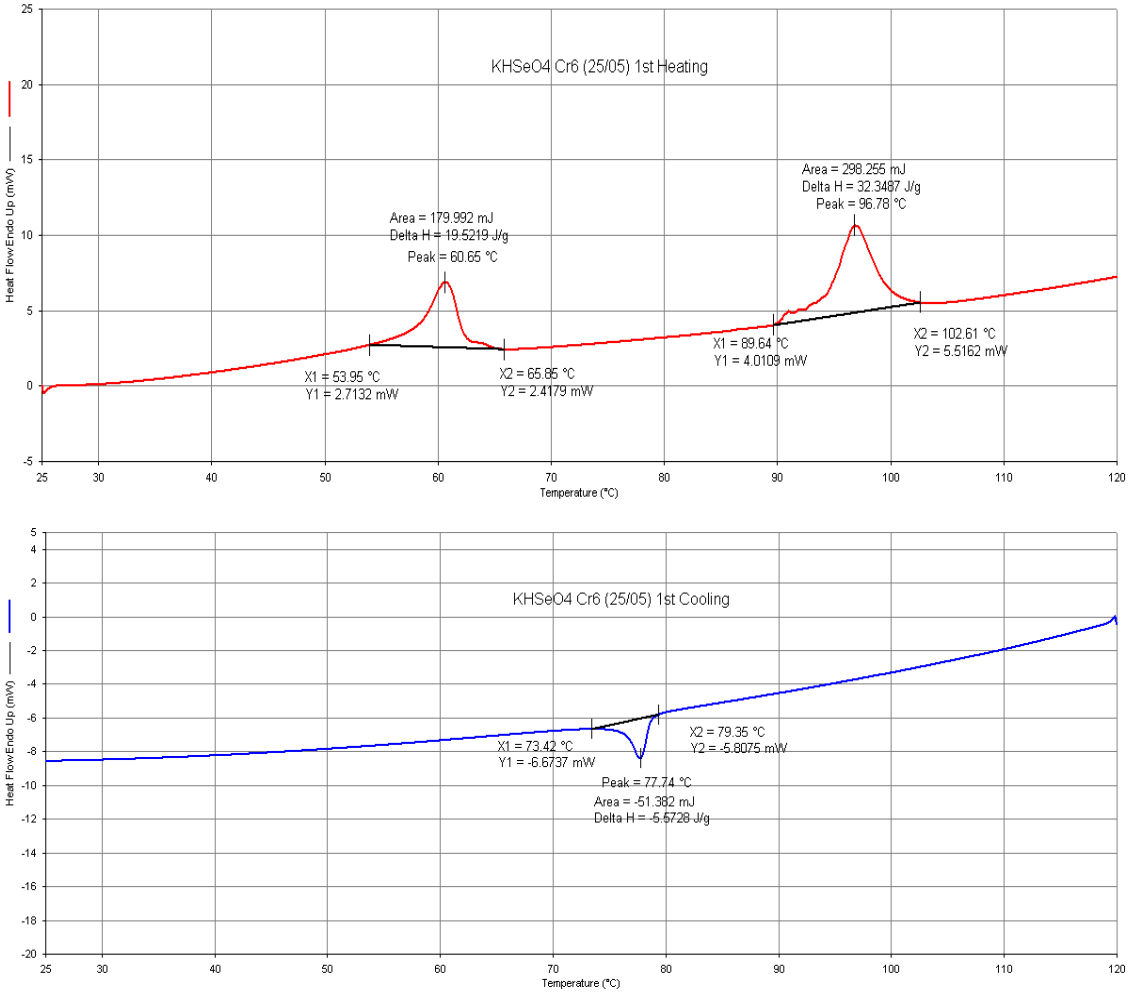

Figure ESI-2. DSC trace of [18-crown-6·K]$HSeO_4$·2H_2O

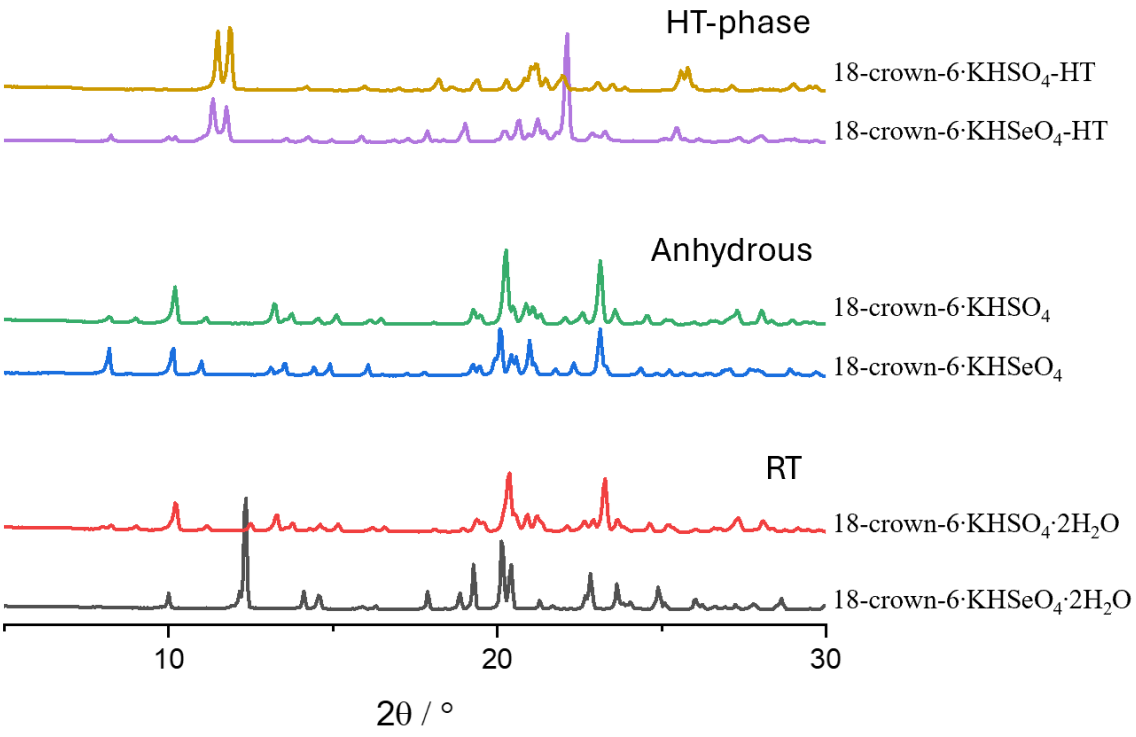

Figure ESI-3. Comparison of the powder patterns of [18-crown-6·K]$HSeO_4$ and 18-crown-6·$KHSO_4$ in increasing temperatures.

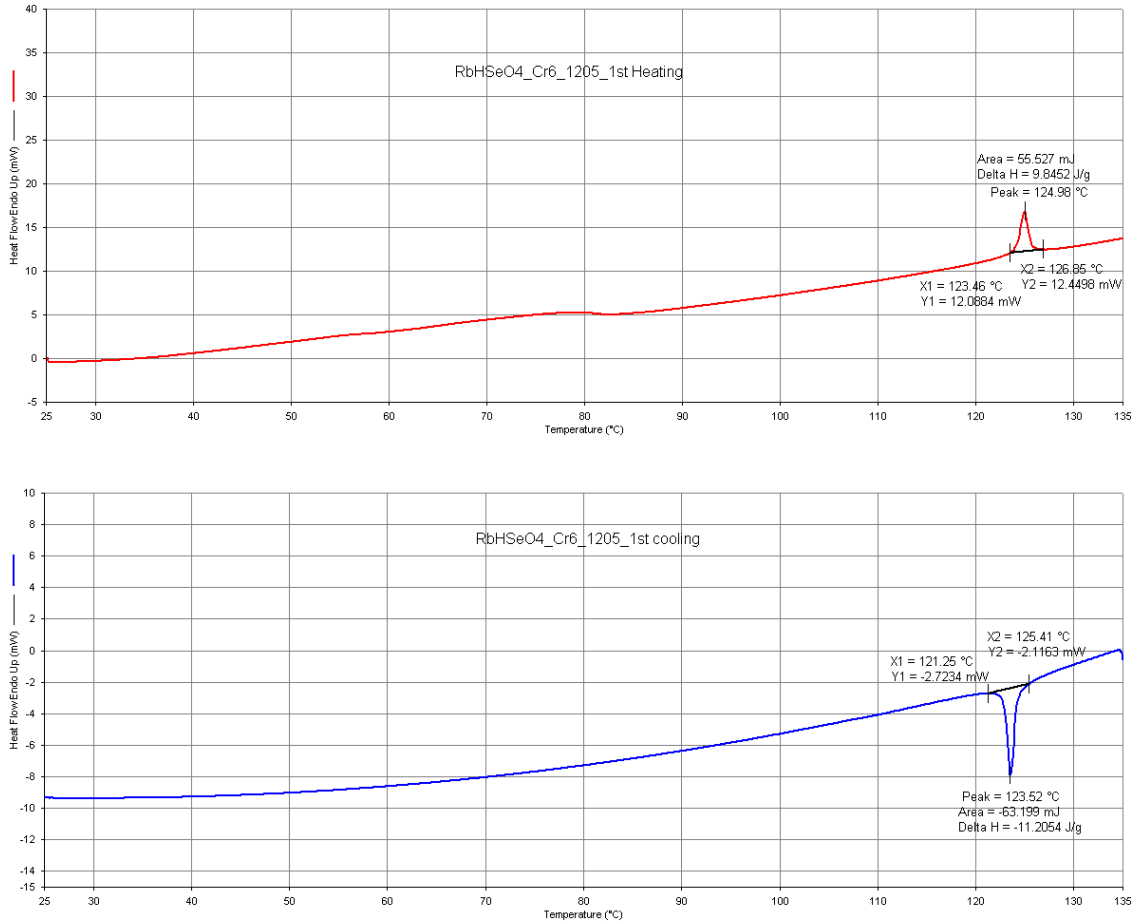

Figure ESI-4. DSC trace of [18-crown-6·Rb]$HSeO_4 \cdot H_2O$

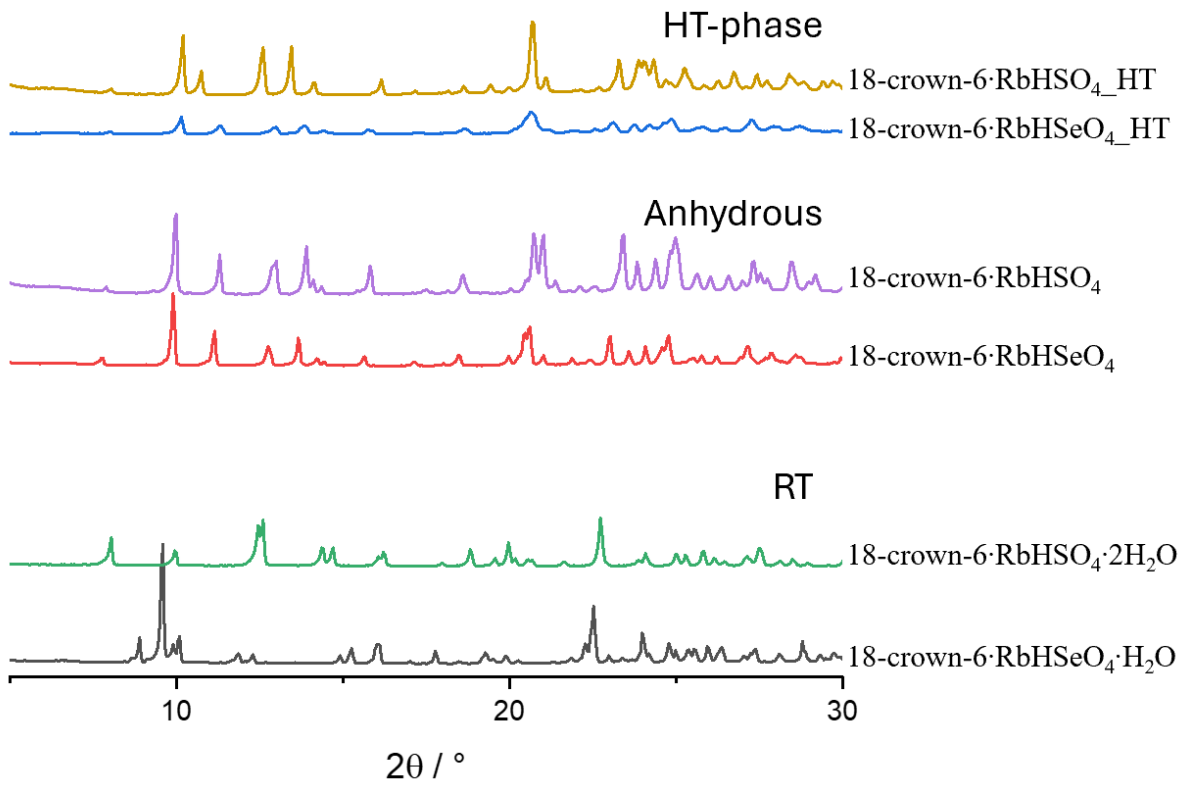

Figure ESI-5. Comparison of the powder patterns of [18-crown-6·Rb]$HSeO_4$ and 18-crown-6·$RbHSO_4$ in increasing temperatures.

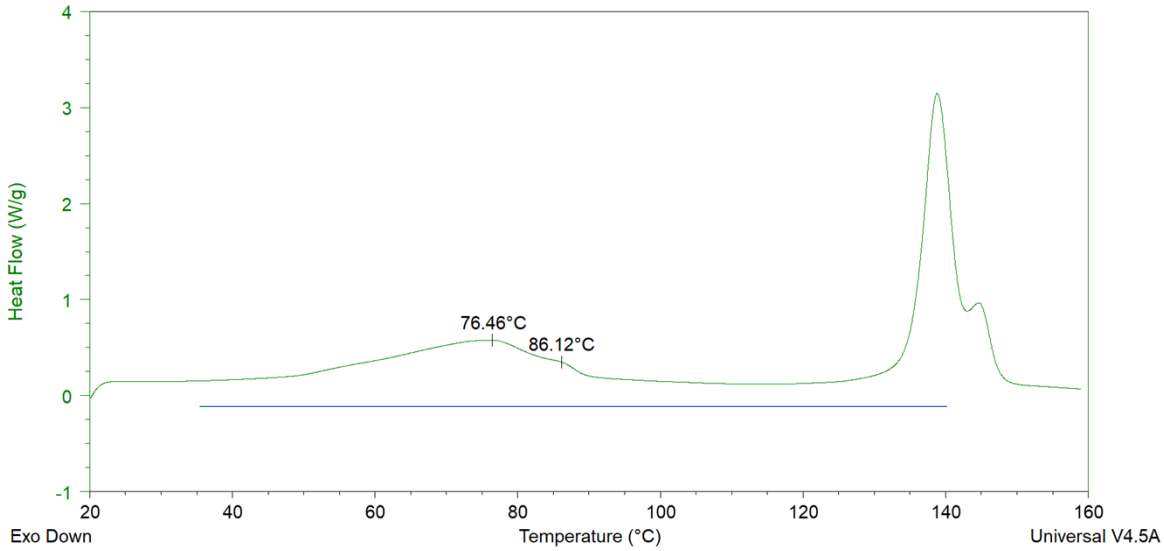

Figure ESI-6. DSC trace of [18-crown-6·Cs]$HSeO_4$·H_2O

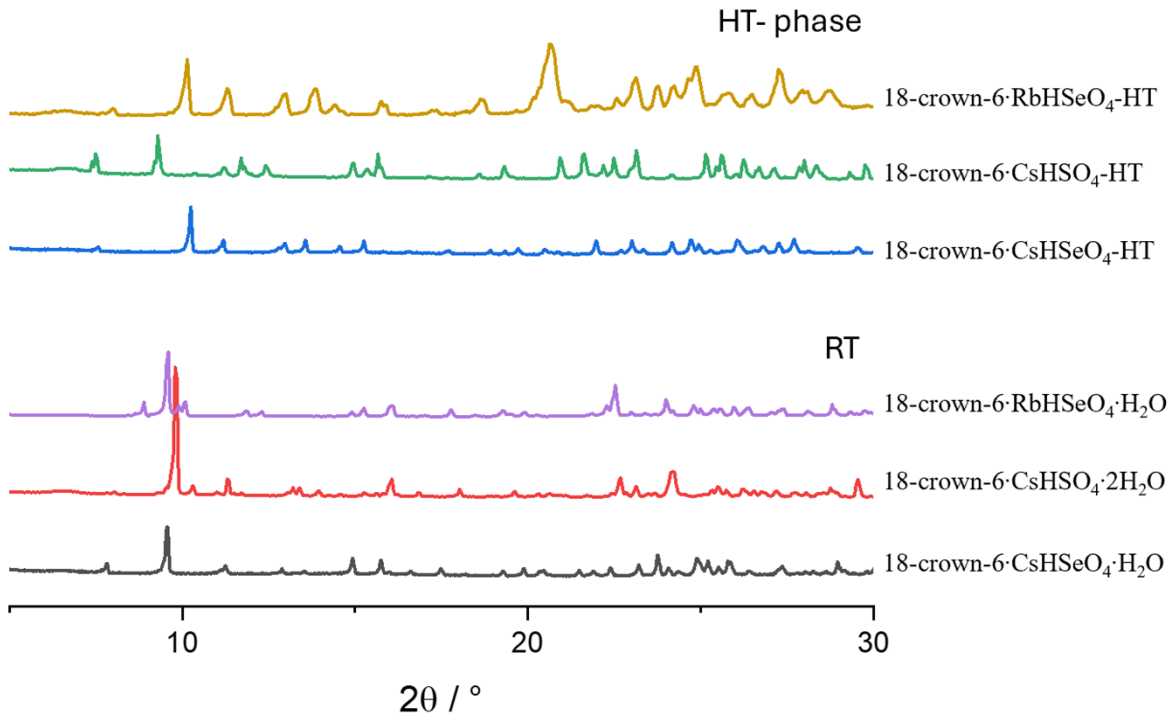

Figure ESI-7. Comparison of the powder patterns of [18-crown-6·$CsHSO_4$], 18-crown-6·$CsHSeO_4$, and 18-crown-6·$RbHSeO_4$ in increasing temperatures.

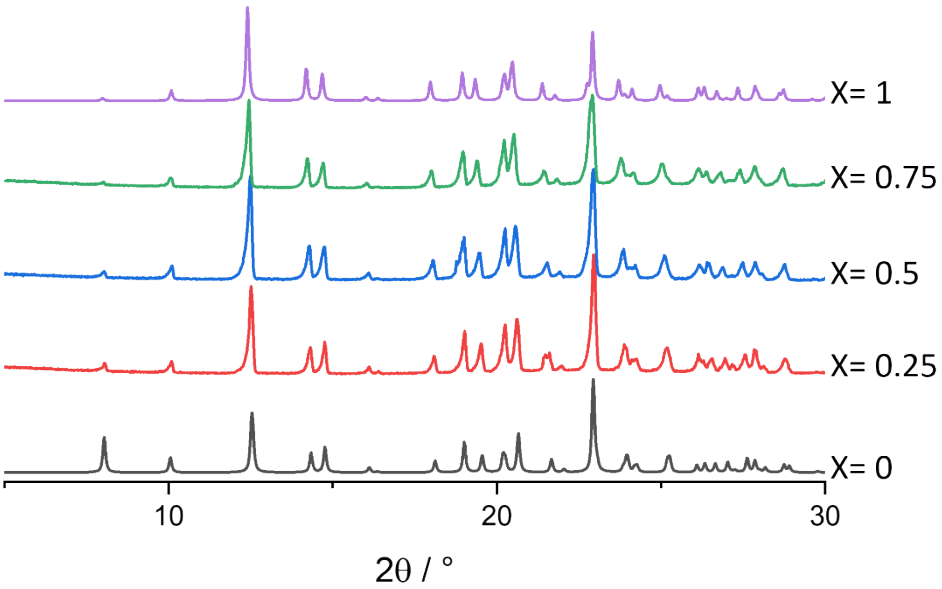

Figure ESI-8. PXRD of [18-crown-6·K]$(HSeO_4)_x(HSO_4)_{1-x}$.

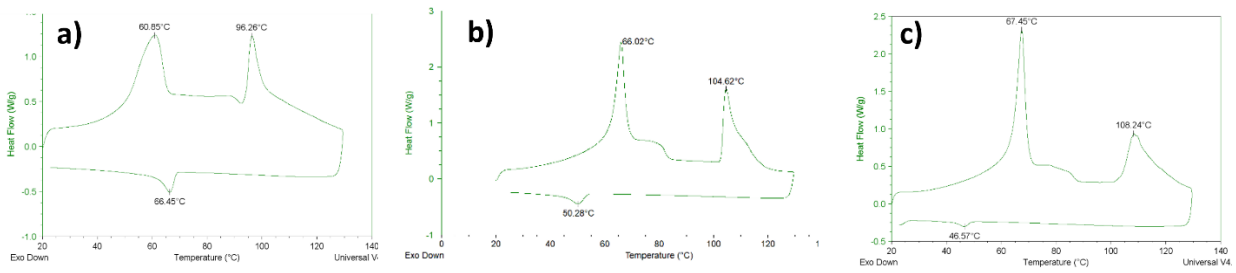

Figure ESI-9. DSC traces of [18-crown-6·K]$(HSeO_4)_x(HSO_4)_{1-x}$. a) x= 0.75, b) x= 0.5, c) x= 0.25.

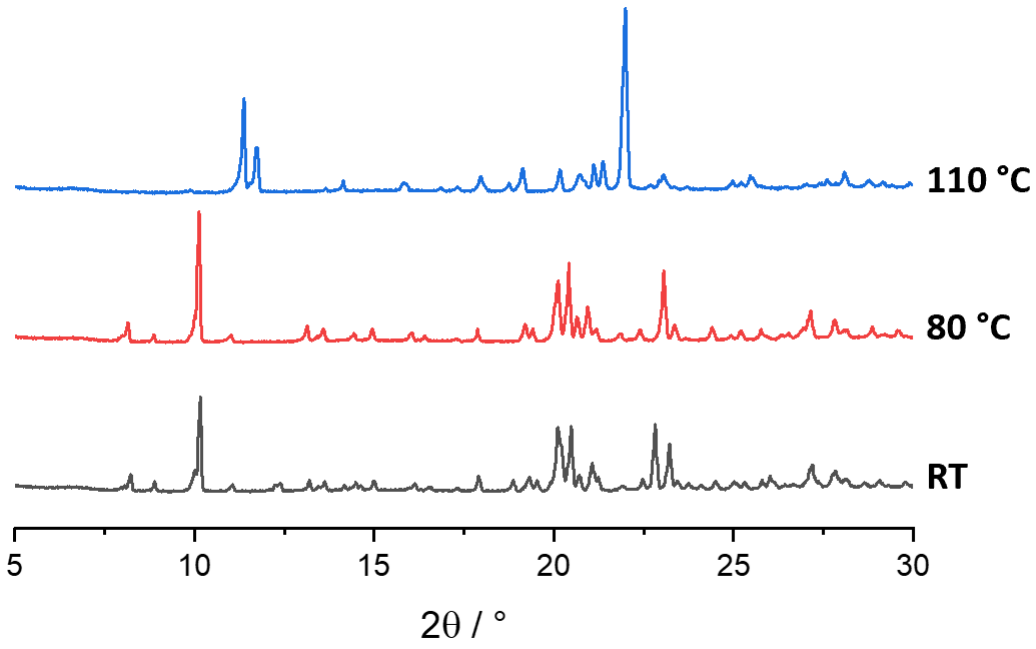

Figure ESI-10. VT-PXRD of 18-crown-6·$K(HSO_4)_{0.5}(HSeO_4)_{0.5}$.

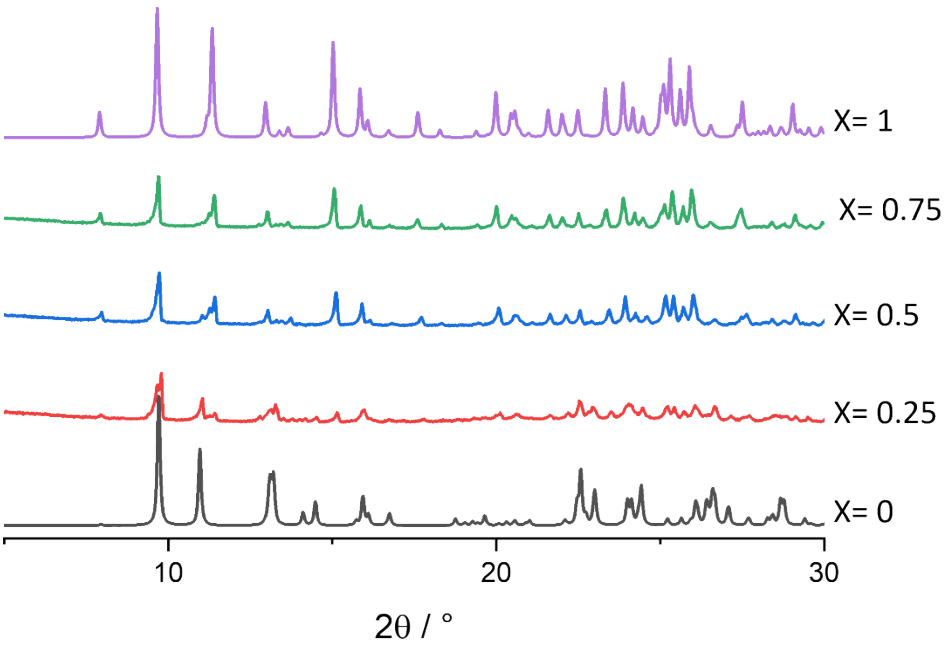

Figure ESI-11. PXRD of [18-crown-6·Cs]$(HSeO_4)_x(HSO_4)_{1-x}$.

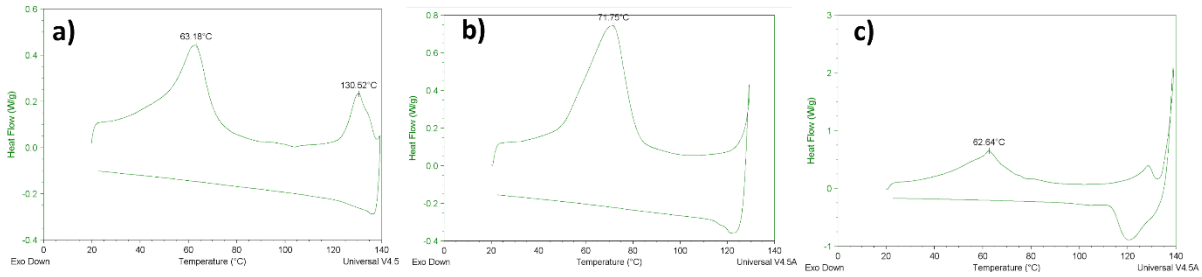

Figure ESI-12. DSC traces of [18-crown-6·Cs]$(HSeO_4)_x(HSO_4)_{1-x}$. a) x= 0.75, b) x= 0.5, c) x= 0.25.

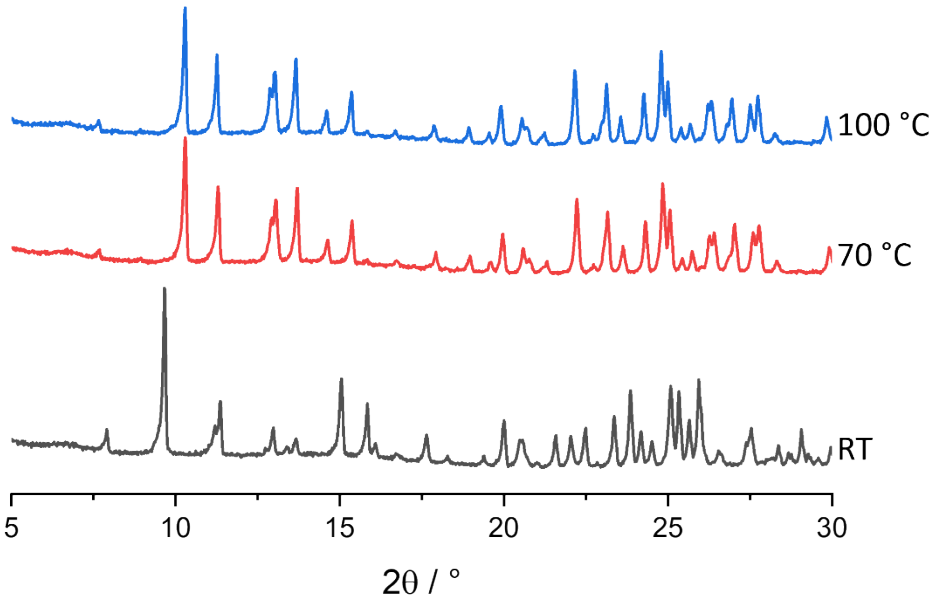

Figure ESI-13. VT-PXRD of 18-crown-6·$Cs(HSO_4)_{0.5}(HSeO_4)_{0.5}$.

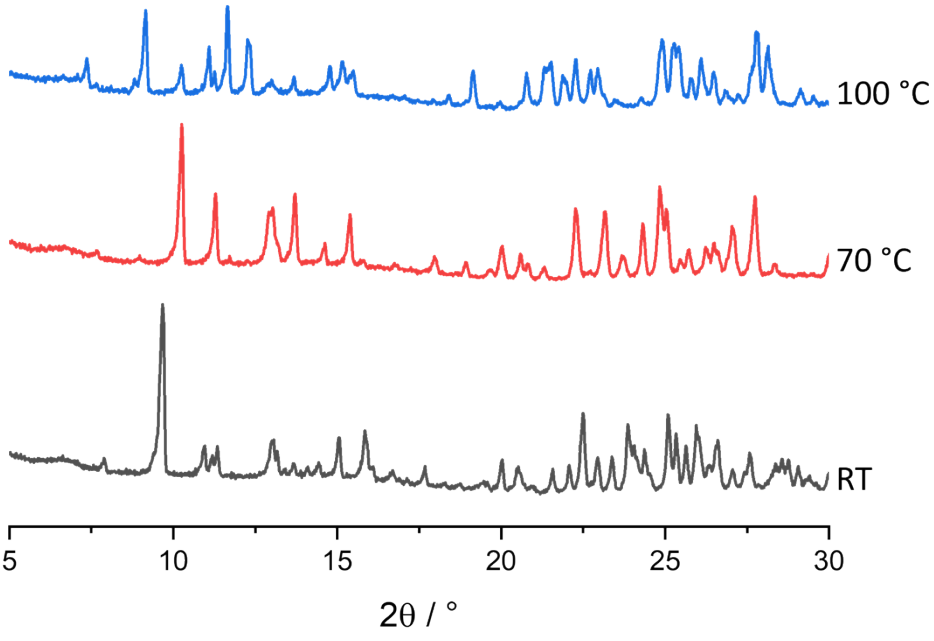

Figure ESI-14. VT-PXRD of 18-crown-6·$Cs(HSO_4)_{0.75}(HSeO_4)_{0.25}$.

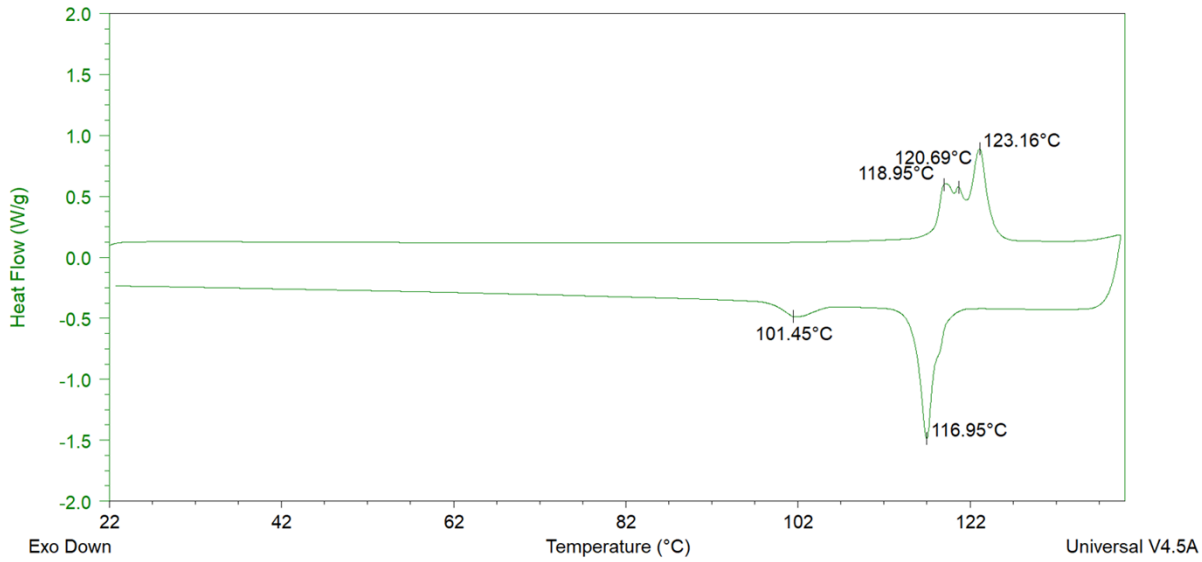

Figure ESI-15. DSC trace of the trial of [18-crown-6·Rb]$(HSeO_4)_{0.5}(HSO_4)_{0.5}$

Table ESI-2. Metal coordination distances and hydrogen bonding interactions detected within crystalline [18-crown-6·K]HSO_4, [18-crown-6·K]$HSeO_4$, and their solid solution [18-crown-6·K]$(HSeO_4)_{0.5}(HSO_4)_{0.5}$.

	[18-crown-6·K]HSO_4	**[18-crown-6·K]$(HSeO_4)_{0.5}(HSO_4)_{0.5}$**	**[18-crown-6·K]$HSeO_4$**
$K^+ \cdots O_{anion}$	2.803(7) - 2.850(7)	2.7403 - 2.9966	2.842(7) - 2.881(7)
H-bond ($O_{anion} \cdots O_{anion}$)	2.561(8)	2.4750 - 2.8815	2.555(8)